17th Anniversary Faculty of Industrial Technology UPH

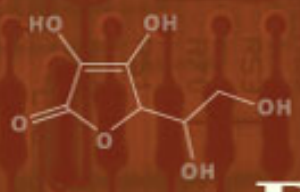

ADVANCES IN ENGINEERING & TECHNOLOGY

Industrial Engineering (Since 1994)
Electrical Engineering (Since 1994)
Food Technology (Since 1995)

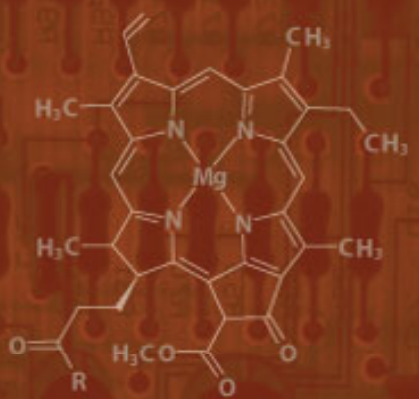

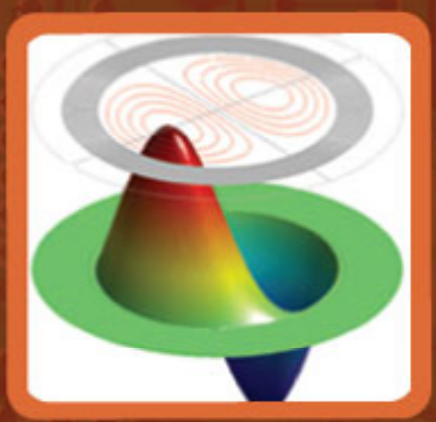

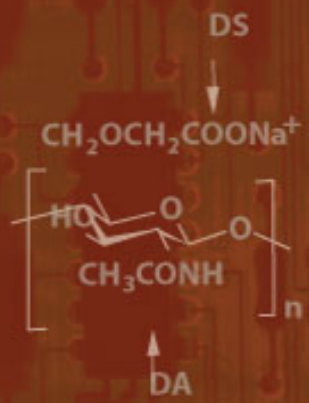

Editors : Ihan Martoyo, Henri P. Uranus, W. Donald R. Pokatong, Jessica Hanafi

UPH
UNIVERSITAS PELITA HARAPAN

Advances in Engineering and Technology

Foreword: Herman Y. Kanalebe

Contributors:

Electrical Engineering Dept. - UPH:
Amelia Redita, Endrowednes Kuantama, Henri P. Uranus, Herman Y. Kanalebe, Ihan Martoyo, Jessie Darma, Junita, Kuniwati Gandi, Leonardy Setyawan, Mario G. Rhizma.

Industrial Engineering Dept. - UPH:
Agustina Christiani, Anthony Riman, Donny Indrawan, Enda Layuk Allo, Eric Jobiliong, George Frahm, Helena J. Kristina, Jessica Hanafi, Joe Kwan Hoei, Laurence, Rudy V. Silalahi, Vicky L. Japhar.

Food Technology Dept. – UPH:
Adolf Parhusip, Anastasia, Hardoko, Lucia C. Soedirga, Melanie Cornelia, Mery T.D. Ambarita, Nuri Arum Anugrahati, Sarmauli I. Manurung, Raniayu, Ratna Handayani, Tagor M. Siregar.

Student Contributors:

Electrical Engineering Dept. - UPH:
Arthur Kusumadjaja, Dede A. Budiman, Eddy Wijanto, Edwin J. Sumadi, Faisal Rahardja, Frederick, Haris Ega, Hendrik, T. Heryanto Wibowo, Leonardus Mario Kesaulja, Margaritifera J.I. Tilaar, Satriya U. Sunarto.

Industrial Engineering Dept. - UPH:
Agus, Andy M. Gunadi, Ferdynando, Jorentius Tanto, Marsha Hidayat, Martinus A. Hendrata.

Food Technology Dept. - UPH:
Clara Fransisca, Ika Narishantika, Novita Rani, Oei Safira Y. Wiharja.

Collaborators: Friedrich K. Jondral (Communications Eng. Lab, Karlsruhe Institute of Tech., Germany), Hery S. Djie (JDS Uniphase Corp, San Jose, USA), H.J.W.M Hoekstra (MESA+, Institute for Nanotechnology, Univ. Twente, The Netherlands), Lina Cahyadi (Mathematics Dept., UPH), Youl-Moon Sung, Dong-Joo Kwak, Doo-Hwan Kim**,** Byungho Kim**,** Jinchun Kim (Kyungsung Univ., Busan, Republic of Korea), Grit Shuster (Berlin, Germany), G.O.F Parikesit (Engineering Physics Dept., Universitas Gadjah Mada, Yogyakarta), A. Sopaheluwakan (Lab-Math Indonesia, Bandung), Karyono (Computer System Dept., Universitas Multimedia Nusantara), Herry Cahyana (Chemistry Dept., Univ. of Indonesia), Joseph R. Powers (Dept. of Food Science & Human Nutrition, Washington State Univ., USA), Leonardus Broto (Research Center for Chemistry, LIPI), Ermiziar (Chemical Eng. Dept., Institut Teknologi Indonesia), Agus Purwanto (STKIP Surya), Rijanto Purbojo, Hendy Wijaya (E-Learning, UPH), Pujianto Yugopuspito (Informatics Dept., UPH).

Editors: Ihan Martoyo, Henri P. Uranus, W. Donald R. Pokatong, Jessica Hanafi.

Cover Design: Anita Suhendro

Tangerang
UPH Press, 2012

Perpustakaan Nasional**:** Katalog Dalam Terbitan (KDT)

Advances in Engineering & Technology /
Authors, Ihan Martoyo ...[et al.].; editors, Ihan Martoyo, Henri P. Uranus, W. Donald R. Pokatong, Jessica Hanafi – Tangerang: Universitas Pelita Harapan Press, 2012. 366 hlm; 29.7 cm.

ISBN 978-979-9103-75-8

Advances in Engineering & Technology
By: Faculty of Industrial Technology, Universitas Pelita Harapan
ISBN 978-979-9103-75-8

Publisher:
Universitas Pelita Harapan Press
Menara UPH
Jl. M.H. Thamrin Boulevard 1100
Lippo Village (Karawaci) – Tangerang 15811 – Indonesia
Tel. 62-21-5460901, Fax. 62-21-5460910

Table of Contents

ARTICLES IN FOOD TECHNOLOGY

ARTICLES IN INDUSTRIAL ENGINEERING

ARTICLES IN ENGINEERING EDUCATION

Leaky Defect Resonance:
How Engineers Turn Defect and Leakage into Powerful Lightguides

H. P. Uranus[1,2,*] and H. J. W. M. Hoekstra[3]
[1]Graduate Program in Electrical Engineering, University of Pelita Harapan,
Plaza Semanggi, Kawasan Bisnis Granadha, Jl. Jend. Sudirman Kav. 50, Jakarta 12930, Indonesia
[2]Department of Electrical Engineering, University of Pelita Harapan,
Lippo Village, Tangerang, 15811, Indonesia.
[3]MESA+ Institute for Nanotechnology, University of Twente, P.O. Box 217,
7500 AE Enschede, The Netherlands.
*e-mail: henri.uranus@uph.edu

***Abstract*- This paper reviews optical structures that utilize mechanism other than the traditional total internal reflection to (quasi-)guide light. Instead, they use the leaky defect-resonance mechanism. Structures with 2-D (i.e. channel waveguides) cross-sections will be studied using a finite element method leaky mode solver. The results will be used to get insights into their properties and principles. Structures being studied include integrated-optical and fiber-optical leaky waveguides, among others are the buffered leaky waveguides, the ARROWs (anti-resonant reflecting optical waveguides), and the photonic crystal fibers. Besides structures that guide light in solid materials, we will also discuss structures that guide light in an air core as well.**

I. INTRODUCTION

This paper discusses structures that use different mechanism than the conventional total internal reflection (TIR) to "guide" [1] light. These structures include integrated-optical and fiber-optical leaky waveguides, like buffered leaky waveguides (i.e. waveguides made on a high index substrate by the help of a low index buffer layer) [2], ARROWs (anti-resonant reflecting optical waveguides) [3], and photonic crystal fibers (PCFs) [4]. Although in their practical forms, structures based on these working principles exhibit inherent confinement losses, they are particularly interesting as they offer several unique properties unattainable by the traditional TIR-based structures. In integrated optics, they can be fabricated using low-cost, widely available semiconductor wafers (which are usually of high refractive index) as substrates, together with the well-developed processing technologies available for them, e.g. those used by the microelectronics industry. For optical fiber, they enable the use of only a single solid material, but open up a larger degree of freedoms in designing, since the properties of the waveguides can now be controlled by the size, shape, orientation, and arrangement of the microstructural air holes [5]. Most of the structures exhibit unusual dispersion properties, which can be utilized for specific applications. They also enable the quasi-guiding of light in an air or liquid core [6], which opens up various new applications regarding very localized light-gas [7], light-liquid [8], or even light-particle interactions [9], both using fiber- or chip-based structures.

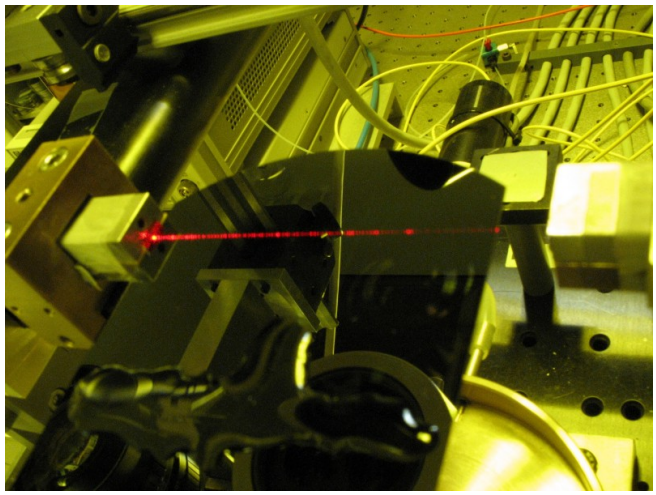

(a)

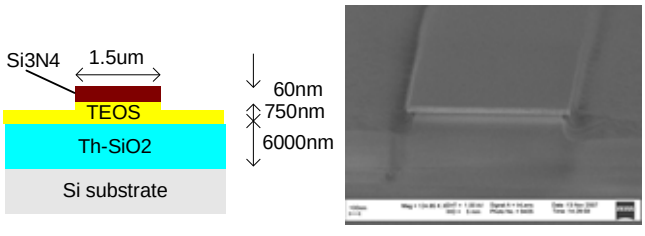

(b) (c)

Fig. 1. (a). Light from a laser at the left is coupled and propagating in a straight waveguide using a low-index Si_3N_4 core grown on a high-index Si substrate. The aimed cross-section of the structure is shown in (b), while the SEM image of realized structure is shown in (c). This buffered leaky waveguide works without the TIR mechanism. TEOS = tetraethyl orthosilicate glass, Th-SiO_2 = thermally oxidized SiO_2.

Fig. 1 shows an example of such structures fabricated at the Univ. Twente. Here, we pick up a rather simple structure called the buffered leaky waveguide. In this waveguide, light

propagates in a straight Si_3N_4 strip waveguide grown on a high-index silicon substrate. While the core of the waveguide was made of material with refractive index of 2, the substrate has refractive index of 3.5. Although the substrate refractive index is higher than that of the core, hence TIR is beyond the reach, such structure can guide light as demonstrated in Fig. 1(a).

We will discuss the principles, modeling, and applications of such structures. We will first discuss the principles of quasi-guiding light by leaky defect resonance, then the modeling method used for our works, and finally review various structures and apply the model to study them.

II. Quasi-Guiding Light by Leaky Defect Resonance

There are many ways to quasi-guide light beyond the TIR mechanism. Photonic crystal e.g. requires photonic band gap [10] induced by periodic structures that inhibits light within certain frequency range to propagate at that region, while creating defect at certain part of the crystal to allow light to propagate only at that particular region. However, since there is no infinite periodic structure in practical devices, there is no true photonic bandgap in practice.

For certain microstructured waveguides like PCFs with solid core, the so called modified TIR [5] is usually considered as its working principle. In this model, the holey cladding is considered to have a lower equivalent refractive index than the solid core, and hence provides a similar light guiding mechanism as in the ordinary fiber. However, the holey cladding normally occupies only a small part of the whole cladding due to mechanical and fabrication-complexity reasons. A large part of the cladding, i.e. the outer cladding, is normally made of the same material as the core. Hence, there is no true TIR or index-guiding mechanism in this case.

One model that we proposed to explain both of the above mentioned quasi-guiding of light is resonance [11]. Resonance is a condition where inhomogenities in the structure creates reflections which interfere constructively in a certain region called the core region. The inhomogenities can be considered as defects with respect to the homogeneous background. Hence, we term this quasi-guiding mechanism as defect resonance. Note that this mechanism is in principle the same as the one that governs the TIR-based waveguide. The difference is simply, here we don't have TIR anymore. Consequently, the waveguide will now suffer from loss. This structural induced loss is known as the confinement loss. Hence, similar modeling methods which are usually used for TIR-based waveguides can be applied here, except now we have to employ boundary conditions which allow light to leak-out. The method will compute for the so-called leaky modes [12] of the structures.

III. FEM Modeling of Quasi-Guiding Light by Leaky Defect Resonance

Lets consider longitudinally-invariant channel waveguide structures as shown in Fig. 2, which is composed of non-magnetic anisotropic materials with diagonal permittivity tensors and $\exp(j\omega t)$ time dependence of the field, where ω is the angular frequency and t is the time. From Maxwell's equations it is possible to derive a magnetic-field-based vectorial wave-equation,

$$\nabla \times \bar{\bar{\varepsilon}}_r^{-1} \nabla \times \vec{H} = k_0^2 \vec{H}, \tag{1}$$

where $\bar{\bar{\varepsilon}}_r$, $\vec{H}$, and k_0 are the material permittivity tensor, magnetic field strength, and freespace wavenumber, respectively. Using Eq. (1), it is possible to get a vectorial wave-equation expressed only in terms of the transverse components of the magnetic field as follows:

$$\begin{bmatrix} \partial_y \left[\frac{1}{n_{zz}^2} \left(\partial_x H_y - \partial_y H_x \right) \right] \\ -\partial_x \left[\frac{1}{n_{zz}^2} \left(\partial_x H_y - \partial_y H_x \right) \right] \end{bmatrix} - \begin{bmatrix} \frac{1}{n_{yy}^2} \partial_x \left(\partial_x H_x + \partial_y H_y \right) \\ \frac{1}{n_{xx}^2} \partial_y \left(\partial_x H_x + \partial_y H_y \right) \end{bmatrix} + k_0^2 n_{\text{eff}}^2 \begin{bmatrix} \frac{1}{n_{yy}^2} H_x \\ \frac{1}{n_{xx}^2} H_y \end{bmatrix} = k_0^2 \begin{bmatrix} H_x \\ H_y \end{bmatrix}, \tag{2}$$

where x, and y are the transversal coordinate of the waveguide as shown in Fig. 2; n_{eff}, ∂_x, and ∂_y are the modal effective index, partial derivative $\partial/\partial x$, and $\partial/\partial y$, respectively. Here, the permittivity tensor is

$$\bar{\bar{\varepsilon}}_r = \begin{bmatrix} n_{xx}^2 & 0 & 0 \\ 0 & n_{yy}^2 & 0 \\ 0 & 0 & n_{zz}^2 \end{bmatrix}, \tag{3}$$

meaning that the crystal anisotropy principal axes coincide with the waveguide coordinate system as shown in Fig. 2.

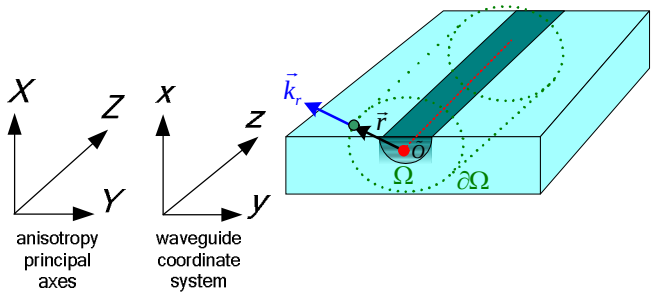

Fig. 2. Coordinate systems used in modeling of channel structures.

We will use the finite element method (FEM) to model the structure. Using the Galerkin procedure [13] and discretizing the computational domain into triangular elements leads to the following discretized weak formulation:

$$\sum_{\substack{BoundaryElement\\ e}} \left\{ -\int_{\Gamma_e} \tfrac{1}{n_{zz}^2} w_y \left(\partial_x H_y - \partial_y H_x\right) dy - \int_{\Gamma_e} \tfrac{1}{n_{zz}^2} w_x \left(\partial_x H_y - \partial_y H_x\right) dx \right.$$
$$\left. -\int_{\Gamma_e} \tfrac{1}{n_{yy}^2} w_x \left(\partial_x H_x + \partial_y H_y\right) dy + \int_{\Gamma_e} \tfrac{1}{n_{xx}^2} w_y \left(\partial_x H_x + \partial_y H_y\right) dx \right\}$$
$$+ \sum_{\substack{InterfaceElement\\ e}} \left\{ -\int_{\Gamma_{int,e}} \tfrac{1}{n_{yy}^2} w_x \left(\partial_x H_x + \partial_y H_y\right) dy + \int_{\Gamma_{int,e}} \tfrac{1}{n_{xx}^2} w_y \left(\partial_x H_x + \partial_y H_y\right) dx \right\}$$
$$+ \sum_{\substack{TriangularElement\\ e}} \iint_{\Omega_e} \left\{ \tfrac{1}{n_{zz}^2} \left(\partial_x w_y - \partial_y w_x\right)\left(\partial_x H_y - \partial_y H_x\right) \right.$$
$$+ \left[\partial_x \left(\tfrac{1}{n_{yy}^2} w_x\right) + \partial_y \left(\tfrac{1}{n_{xx}^2} w_y\right) \right] \left(\partial_x H_x + \partial_y H_y\right)$$
$$\left. + k_0^2 n_{eff}^2 \left(\tfrac{1}{n_{yy}^2} w_x H_x + \tfrac{1}{n_{xx}^2} w_y H_y\right) - k_0^2 \left(w_x H_x + w_y H_y\right) \right\} dx\, dy = 0 \quad (4)$$

with w_x and w_y denoting the weight functions, Ω_e the area in each triangular element, $\Gamma_{int,e}$ the line element at the interface between different materials, and Γ_e the line element at the computational boundaries.

Approximating the fields using quadratic nodal-based basis functions

$$H_\eta^{(\Gamma e)} = \sum_{i=1}^{3} N_{i,1D}^{(\Gamma e)} H_{\eta,i}^{(\Gamma e)} \quad \text{for each boundary line element } \Gamma_e,$$

$$H_\eta^{(\Gamma \mathrm{int},e)} = \sum_{i=1}^{3} N_{i,1D}^{(\Gamma \mathrm{int},e)} H_{\eta,i}^{(\Gamma \mathrm{int},e)} \text{ for each interface line element } \Gamma_{int,e},$$

$$H_\eta^{(e)} = \sum_{i=1}^{6} N_{i,2D}^{(\Omega e)} H_{\eta,i}^{(\Omega e)} \quad \text{for each triangular element } \Omega_e, \quad (5)$$

where $\eta = x,y$; while $N_{i,1D}$ and $N_{i,2D}$ denoting the quadratic 1-D and 2-D basis functions, respectively with i denoting the local nodal points within the corresponding element; we can write the approximation to Eq. (4) into a sparse generalized eigenvalue equation as follows:

$$\left(\mathbf{M}_1 - n_{eff}^2 \mathbf{M}_2\right)\{H\} = \{0\}, \quad (6)$$

with column vector $\{H\}$ representing the approximate H_x and H_y fields at nodal points, while $\{0\}$ is a null vector. The matrices $\mathbf{M}_1$ and $\mathbf{M}_2$ are sparse and have the dimension of only $2N$ X $2N$, with N denoting the number of nodal points. Eq. (6) can be solved using an eigenvalue solver to obtain the eigenvalues related to the modal indices (n_{eff}) and eigenvectors associated with the transverse components of the magnetic field of the corresponding modes.

The derivatives of the fields occurring in the boundary term in Eq. (4) will be handled through a 1st-order BGT-like [14] transparent boundary conditions (TBC) to mimic the properties of the fields in the exterior domain properly. For this purpose, we use a vector radiation function

$$\vec{H}(r,\theta)\big|_\Gamma = \begin{bmatrix} H_x \\ H_y \end{bmatrix}\Big|_\Gamma = \sum_{p=0}^{\infty} \frac{1}{r^{p+1/2}} \begin{bmatrix} H_{x,p}(\theta)\exp\left(-jk_{r,x}r\right) \\ H_{y,p}(\theta)\exp\left(-jk_{r,y}r\right) \end{bmatrix} \quad (7)$$

along the computational boundary Γ, which leads to a 1st-order operator on the boundary fields as follows:

$$B_1\left(\begin{bmatrix} H_x \\ H_y \end{bmatrix}\right)\Big|_\Gamma = \left\{ \left(\partial_r + \frac{1}{2r}\right)\begin{bmatrix} H_x \\ H_y \end{bmatrix} + j\begin{bmatrix} k_{r,x} H_x \\ k_{r,y} H_y \end{bmatrix} \right\}\Big|_\Gamma = O\left(r^{-5/2}\right). \quad (8)$$

In Eqs. (7) and (8), r and θ are the polar coordinates of the cross-section whereby the center of the core of the waveguide has been taken as the origin, and $k_{r,x}$ and $k_{r,y}$ are the complex transverse wavenumbers associated with the x and y components of the field. Solving the wave-equation at the elementwise homogeneous anisotropic exterior domain leads to $k_{r,x}\big|_\Gamma = k_0\sqrt{n_{xx}^2 - n_{eff}^2}\Big|_\Gamma$ and $k_{r,y}\big|_\Gamma = k_0\sqrt{n_{yy}^2 - n_{eff}^2}\Big|_\Gamma$ with $\mathrm{Re}(k_r)>0$ associated with the outward leaking case (the leaky-mode case) and $\mathrm{Im}(k_r)<0$ associated with evanescently decaying case (the guided-mode case). By neglecting the angular dependence of the field at each line element, a Dirichlet to Neumann (DtN) map

$$\partial_n H_x\big|_\Gamma = -\hat{r}\bullet\hat{n}\left(jk_{r,x} + \frac{1}{2r}\right)H_x\Big|_\Gamma + O\left(r^{-5/2}\right) \quad (9)$$

$$\partial_n H_y\big|_\Gamma = -\hat{r}\bullet\hat{n}\left(jk_{r,y} + \frac{1}{2r}\right)H_y\Big|_\Gamma + O\left(r^{-5/2}\right) \quad (10)$$

can be obtained and used for approximating the derivative operators within the boundary terms of Eq. (4), hence allowing a proper truncation of the FEM mesh. In Eqs. (9) and (10), n denotes the normal direction, while the carret ("^") symbol denotes unit vector.

Note that, application of boundary conditions induces non-linearity to the eigenvalue problem due to the appearance of n_{eff} (the eigenvalue itself) within the DtN. In this work, we have employed linearization by simple iteration technique to enable the use of linear eigenvalue solver and search only for eigenvalues (n_{eff}) of interest, i.e those related to low-loss, localized leaky modes within the expected effective index range.

IV. Review on various leaky waveguides

IV.1. Quasi-guiding Light in Solid-core Waveguides

IV.1.1. Buffered Leaky Waveguides

Optical waveguides made on a semiconductor substrate are widely used. They gain advantages from the wide availability of such substrates. Besides, they also share the well-developed processing technologies being used also by other disciplines, like the well-established microelectronics industry. Among these are the waveguides made on the low-cost silicon substrate. Unfortunately, the refractive index of this substrate is high, while materials which are compatible with this substrate and suitable for guiding light, like silicon oxynitride (SION), silicon nitride, silica, or silicon itself have lower or the same refractive index. A way to deal with this

circumstance is by putting another lower refractive index material between the waveguiding structures and the high-index substrate as shown in Fig. 3. This so-called buffer layer acts as a buffer that isolates the light in the waveguiding structures from the substrate. Besides waveguides made on high-index substrates, the existence of a high-index component in the proximity of an ordinary waveguide also creates a buffered leaky waveguiding structure. Such situations occur in case of a prism-loaded waveguide [15], a waveguide tuned by high-index material overlaid on top of it, or an optical MEMS movement sensor [16]. In the last three cases, either air or index-matching oil can be regarded as the buffer layer. These structures are apparently leaky, as the light prefers to travel into the high-index substrate. However, as is already well known, if this layer is thick enough, the confinement loss of the structure can be small enough to allow functional integrated optical circuits to be built based on this approach [17].

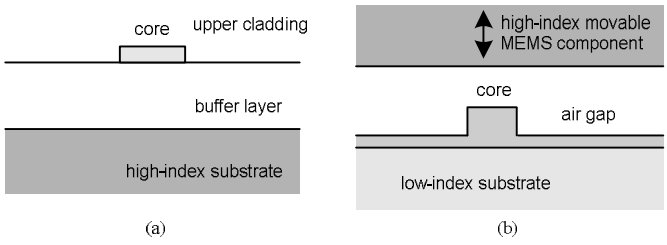

Fig. 3. Examples of buffered leaky waveguides: (a). strip waveguide made on a high-index substrate and (b). an optical MEMS movement sensor.

The silicon on insulator (SOI) waveguides are examples of buffered leaky waveguides. SOI waveguides are made on a thin Si core channel sitting on a SiO_2 buried oxide (BOX) layer on top of a high-index silicon substrate. Recently, SOI is getting more popular, since the high refractive index of silicon enables the realization of nanometric photonic wire [18] which enables sharp bends. Hence, SOI technology is prospective for realization of complicated circuits on small wafer footprint. Moreover the device can be realized using industry-standard CMOS-compatible, deep-UV wafer-stepping technologies. Researchers around the world are still working hard toward reduction of sidewall scattering loss in order to get a reasonable loss for functional devices.

Fig. 4 illustrates a FEM model of a SOI strip waveguide [19]. The triangles denote the discretization mesh of the structure. Due to the structural symmetry, only half of the structure is required in the model by the application of symmetry boundary conditions [11]. We have taken finer mesh at around the core where the modal fields are stronger. By taking parameters from a commercial SOI wafer with BOX thickness t_b = 2 μm, core thickness t = 220 nm, and core width of w = 700 nm, and by putting water as the upper cladding (which is of interest of sensing applications), and using the method described in Section III, we obtained 3 low-loss leaky modes with profiles plotted in Fig. 5. Hereafter, the "q" letter in front of the mode label denotes "quasi" as modes in rectangular channel waveguides are vectorial (not truly linearly polarized). Table 1 shows that by reducing the width of the strip, the real part of the modal index getting lower, meaning that the modes become less confine (as shown in Fig. 6) and correspondingly the confinement loss gets higher. This fact can be used to tune the number of dominant modes. Since leaky waveguides are inherently multimoded [11], the highly leaky modes are automatically rejected during the mode solving iterations, and hence not shown here.

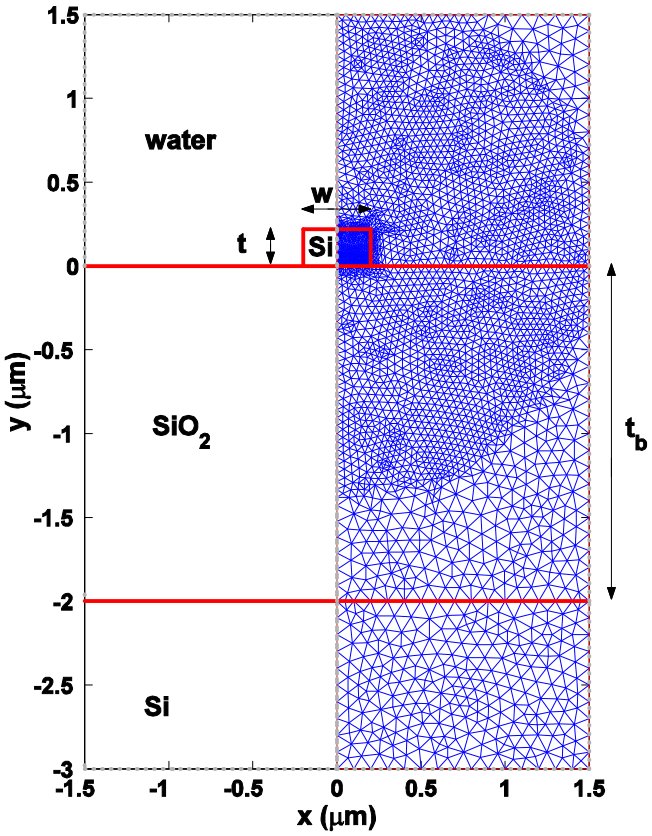

Fig. 4. FEM model of a SOI waveguide. Due to the symmetry of the structure, only half of the structure is needed in FEM modeling. The triangular element discretization of the structure is shown.

TABLE I
DOMINANT MODES OF THE SOI WAVEGUIDES WITH VARIOUS STRIP WIDTH. THE STRIP THICKNESS AND BUFFER LAYER THICKNESS ARE AS IN THE TEXT.

Strip width w (nm)	q-TE_{00}		q-TM_{00}		q-TE_{10}	
	Re{n_{eff}}	α dB/cm	Re{n_{eff}}	α dB/cm	Re{n_{eff}}	α dB/cm
400	2.2001	8.02E-8	1.6315	1.57E-1	-	-
500	2.4312	7.7E-10	1.7124	1.38E-2	-	-
600	2.5573	7.35E-10	1.7733	2.62E-3	1.6338	9.11E-3
700	2.6355	1.78E-11	1.8160	7.95E-4	1.9292	7.13E-6

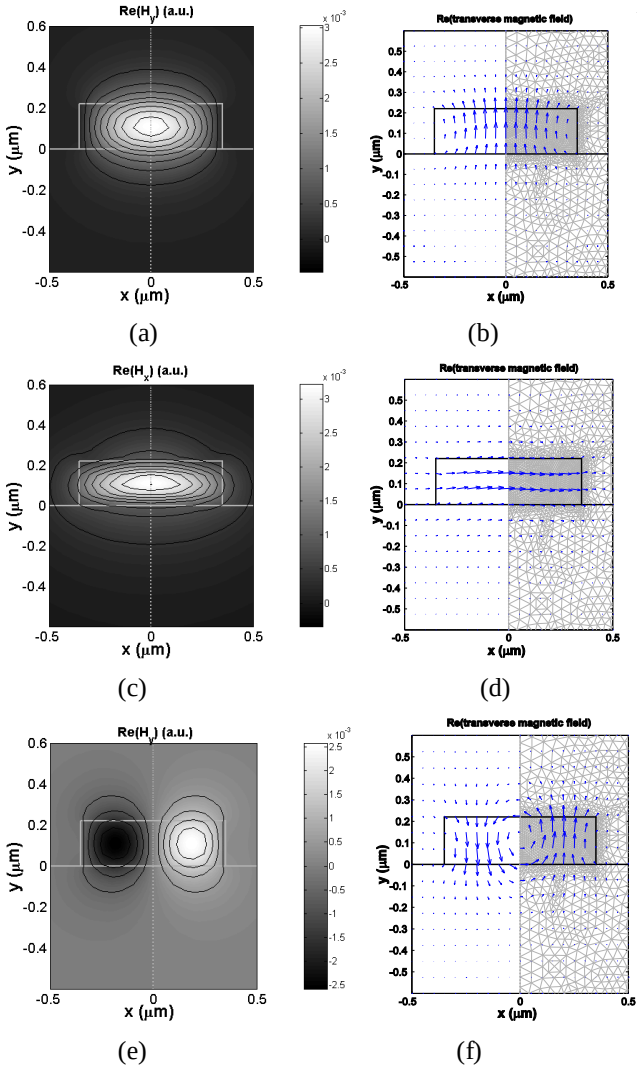

(a) (b) (c) (d) (e) (f)

Fig. 5. The profile of dominant magnetic field component of modes (at the left column) and related transverse magnetic field vector (at the right column) of a SOI strip waveguide with core width w = 700nm, thickness t = 220nm, and buried silica buffer thickness t_b = 2μm with water cladding at wavelength of 1.55μm. (a) & (b) q-TE_{00}, (c) & (d) q-TM_{00}, and (e) & (f) q-TE_{10} modes.

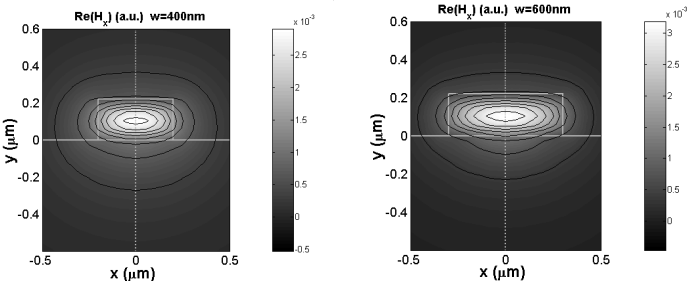

(a) (b)

Fig. 6. Evolution of modal field of q-TM_{00} modes of SOI waveguide with strip width of (a). 400 nm and (b). 600nm. Wider strip will result in more confined mode which corresponds to lower confinement loss.

IV.1.2. ARROWS

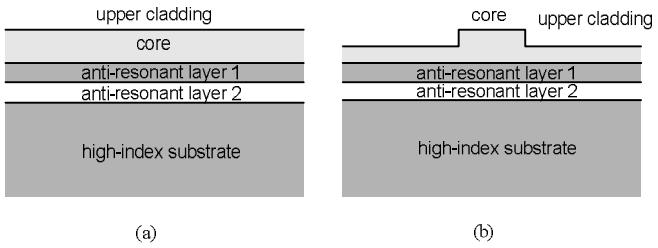

(a) (b)

Fig. 7. (a). A planar and (b) a rib ARROW where cladding bilayers operating in anti-resonant condition suppress the leakage of light from the waveguiding structure into the substrate.

A more advanced way to reduce the leakage of energy from the waveguiding structures into the high-index substrate was proposed by Duguay *et al.* [3] by putting a high and a low refractive index cladding (bi)layers of well-chosen thicknesses between the waveguiding structures and the high-index substrate as illustrated in Fig. 7. These cladding bilayers behave as Fabry-Perot (anti-)resonators operating in the anti-resonant condition, hence exhibiting a very high reflection for the mode of interest, and suppressing the energy leakage into the high index substrate. Based on the way they quasi-guide light, these structures are called the *a*nti-*r*esonant *r*eflecting *o*ptical *w*aveguides (ARROWs). The thicknesses of the cladding layers are designed such that the corresponding layers obey the anti-resonant condition for a transverse wavenumber as follows.

$$2k_{t,i}d_i = 2\pi\left(M + \tfrac{1}{2}\right) \qquad (11)$$

where $k_{t,i}$ and d_i denote the transverse wavenumber and the thickness of cladding layer i, while M = 0,1,2,… denotes the order of the anti-resonance. It is clear that in the design, this anti-resonant condition is associated with one mode (usually the fundamental TE mode) of interest only through the transverse wavenumber. For other higher order modes, these

cladding layers are expected to operate not in the anti-resonant condition, hence exhibiting low reflection and consequently, high confinement loss. However, some higher order modes may still operate in the anti-resonant condition in one of the layers but might be not in the other one; hence, their overall anti-resonant condition is not optimal, leading to higher loss than the fundamental mode. Therefore, there is loss discrimination between modes, which allows the ARROW to be regarded as effectively single-moded if the difference of losses between the mode of interest and the higher order modes are large enough.

ARROWs have been widely used for various applications including sensors [20], splitters [21], spot-size converters [22], etc. Analytical approximate formulae for calculating the thickness of the anti-resonant layers and the losses of the fundamental mode [3], [23] are available and have been widely used, but will most likely be suitable only for planar structures. Hence, rigorous modeling as described in Section III of this chapter will be of importance for channel structures. Surprisingly, the concept of ARROWs, which is relatively simple, can be used to understand part of phenomena appearing in photonic bandgap fibers [24]. In addition to solid core ARROWs, recently hollow-core ARROWs have also been proposed [6]. These structures will be further discussed in Subsection IV.2.2 where low loss hollow core waveguides with rectangular core shape will be an issue.

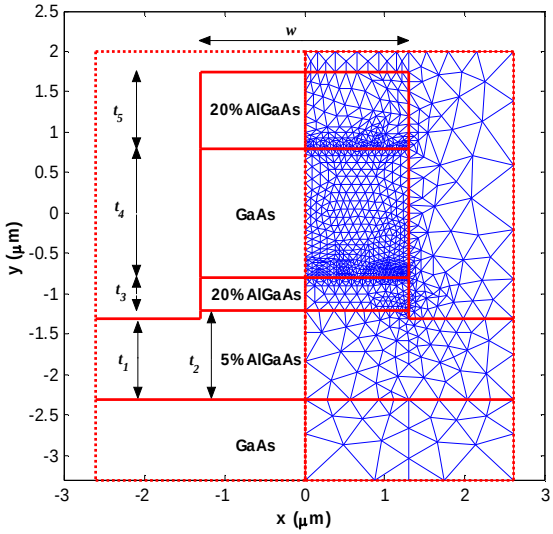

Fig. 8. The structure, computational window, and mesh definition of the rib ARROW.

As an example of an ARROW, we present the mode of a rib ARROW made by a double-heterostructure of III-V compound semiconductor. The structure and the mesh definition of the waveguide are depicted in Fig. 8. The refractive index of the GaAs, 5% AlGaAs, 20% AlGaAs, and air are 3.59, 3.555, 3.452, and 1, respectively. The thicknesses t_1 to t_5 are 1 μm, 1.1 μm, 0.4 μm, 1.6 μm, and 0.95 μm, respectively. The width of the rib is w = 2.6 μm. The operating wavelength is λ = 1.064 μm. The high index substrate causes the waveguide to be leaky. Our computations were carried out using only half of the structure with the computational boundaries located at 1 μm below the substrate-lower-2nd-cladding interface, 0.25 μm above the top of the rib, and 2.6 μm to the right of the symmetry line. Fig. 9 shows the mode profile of the real part of the dominant field of a few modes. For modes with sufficiently large loss, the wave-like tail that indicates leakage into the high-index substrate becomes more noticeable.

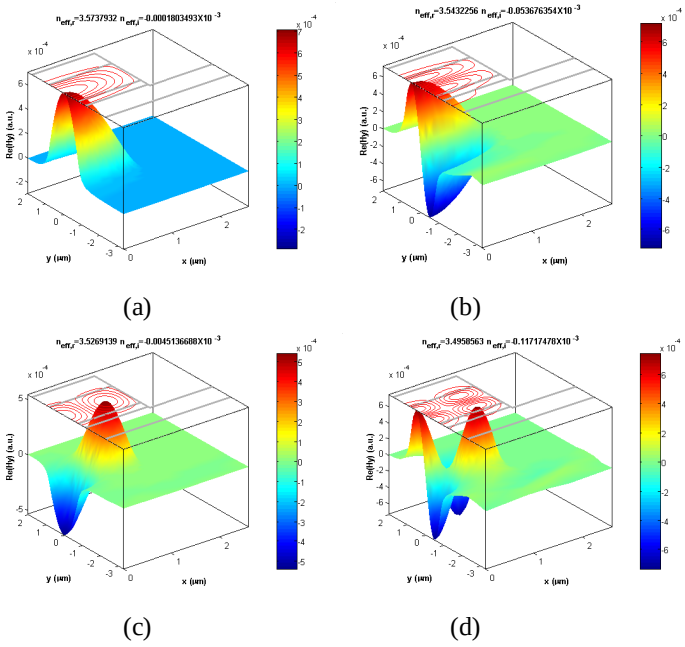

Fig. 9. Mode profiles of the real part of dominant magnetic field component for leaky (a). q-TE_{00}, (b). q-TE_{01}, (c). q-TE_{20}, and (d). q-TE_{21} modes of the rib ARROW.

IV.1.3. High-index-core Photonic Crystal Fibers

Photonic crystal fibers (PCFs) are fibers with a cladding composed of microstructural inclusions running parallel with the propagation axis. In general, the microstructural features are voids (air holes), but in principle, either solid [25] or liquid [26] microstructural features can also be realized. Fig. 10 illustrates some possible PCF structures. Since the idea originated from the use of 2-D photonic crystal to confine light within the core [5], they are popularly referred to as photonic crystal fibers. Unfortunately, later on the community realized, that not all of them work on the basis of the photonic band-gap principles. However, since the name was already widely used, people still keep the same name and add new names to distinguish specific classes of these fibers. Several alternate names have also been given by different research groups to these fibers; e.g. holey fibers, microstructured optical fibers, or crystal fibers. Despite of the

existence of these diversity of names, we will use the term high-index-core PCFs to denote the fibers working on the basis of the leaky defect resonance [27] principles (Fig. 10.(a)-(c)) and photonic bandgap fibers (PBFs) to denote those based on the photonic bandgap principles (Fig. 10.(d)-(f)). One specific type of the PBF, which uses coaxial Bragg reflectors in the cladding will be called as Bragg fiber (Fig. 10.(f)). Meanwhile, the term *PCF* will be used as a universal name to denote all of them. The above terms are widely used by the community [5]. In general, high-index-core PCFs have a solid core, and PBFs have a hollow-core; but in principle, it is also possible to make a PBF with solid core or a leaky-defect-resonance PCF with a non-solid core.

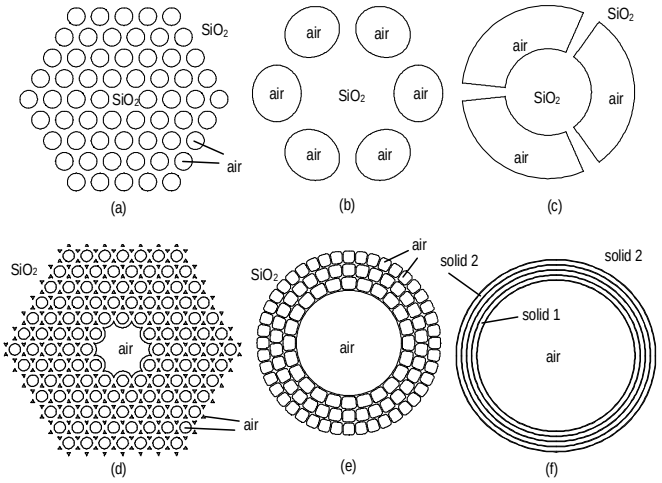

Fig. 10. Examples of cross-section of photonic crystal fibers with (a). high-index core with circular, (b). elliptical, and (c). annular-sector-shaped holes in the cladding; the photonic bandgap fibers with (d). circular and interstitial, (e). annular-sector-shaped holes in the cladding, and (f). the Bragg fiber.

Since the fabrication of the first PCF was demonstrated [4], they have attracted a lot of scientific and commercial interests. Since they allow the use of only a single solid material, they relieve the engineer from the restriction caused by thermal/mechanical incompatibility of different solid materials. However, they allow a new way to engineer the fiber through their geometrical parameters; where the size, shape, orientation, position, and arrangement of the microstructural features are manipulated to tailor their properties. This way of engineering apparently offers more degrees of freedom to the designer. Many new properties unattainable through ordinary fibers can be obtained by this class of fibers. These include fibers with properties like single-modedness over a wide wavelength range [28] while still offering a large mode field diameter [29], zero-dispersion wavelength down to the visible wavelength [30], ultra-flat and ultra-low dispersion [31] or highly negative-dispersion [32] at long-wavelength telecommunication window, fibers with relatively high [33] or low [35] non-linearity, fibers with high birefringence but low temperature-sensitivity [34], etc.

The simple model that is widely used to explain the light "guiding" mechanism in the high-index-core PCF is the so-called modified total internal reflection or the index-guiding model [5]. In this model, the presence of holes will lower the effective refractive index of the holey cladding, hence leads to an equivalent structure with a high-index core surrounded by a low-index cladding, which will guide light losslessly in a similar way as the ordinary fiber. However, the practical PCFs usually have limited size of the holey cladding section, which is surrounded by a large section of uniform high-index outer cladding. Apparently, this situation will lead to a leaky structure. Therefore, the term modified total internal reflection or index-guiding is not accurate [27]. Instead, we will refer their quasi-guiding mechanism to the resonance mechanism. Within this picture, we can consider the holey section of the cladding together with the core as a kind of defect in the background of a uniform high-index outer cladding, hence it can be considered simply as a resonance center, within which the light will be quasi-trapped. Therefore, we can simply call this quasi-guiding mechanism as a defect resonance. In the PCF, since there is no TIR (which would need a lower cladding than core index) and no perfect photonic band gap (which would need a periodic structure extending to infinity) to prevent the leakage of light from the resonant center, we will also observe the presence of leakage or confinement loss. This quasi-guiding mechanism can be applied to understand both the high-index-core PCF and the PBF. In the light of this notion, it is very intuitive to understand the existence of the ordinary-fiber-like core modes, cladding- and core-cladding resonance modes [36], and also the so-called surface modes [37] in the PBF.

Fig. 11.(a) shows a commercial photonic crystal fiber type LMA-15 produced by NKT Photonics [38], while Fig. 11.(b) shows a FEM model of this fiber. Note that by taking advantage of the symmetry of the structure, only a quarter of the structure is sufficient in the model. Fig. 12 shows several dominant calculated modes of the fibers for wavelength of 632.8 nm. Note that this wavelength is not usual in silica fiber applications as it is not located at low-loss windows of silica fiber. The interesting aspect of putting results at this wavelength here is simply because this wavelength is associated with He-Ne laser, which is available at most laboratory and the results shows that there are higher order modes with relatively low confinement loss [39] opposing to the factory's claim [38] that this fiber is endlessly single-mode. Hence it will be interesting to experimentally verify these contradictive hypotheses in the future.

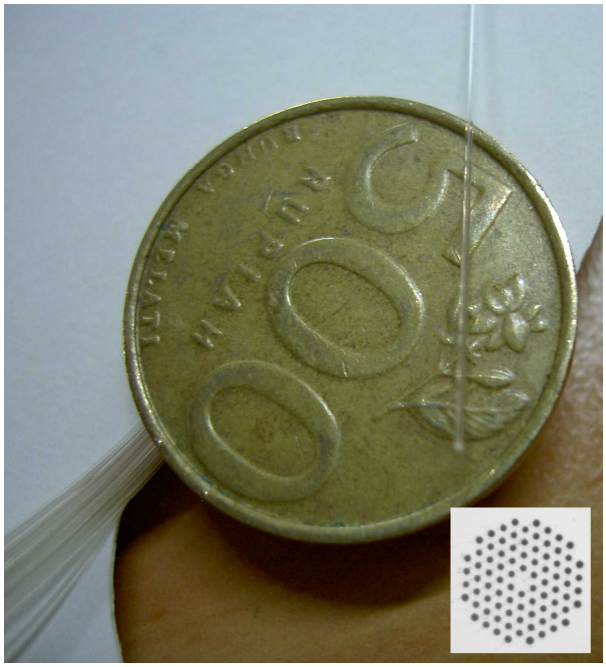

(a)

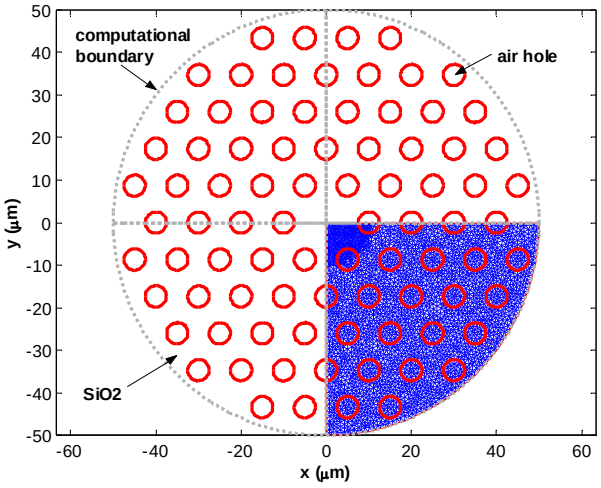

(b)

Fig. 11. (a). A bare commercial PCF of type LMA-15 where the inset shows microstructured holes arranged around its core. Please compare the size of the fiber together with its plastic buffer of 405 μm diameter and an Indonesian coin. (b). The FEM model of the PCF which takes only a quarter of the structure.

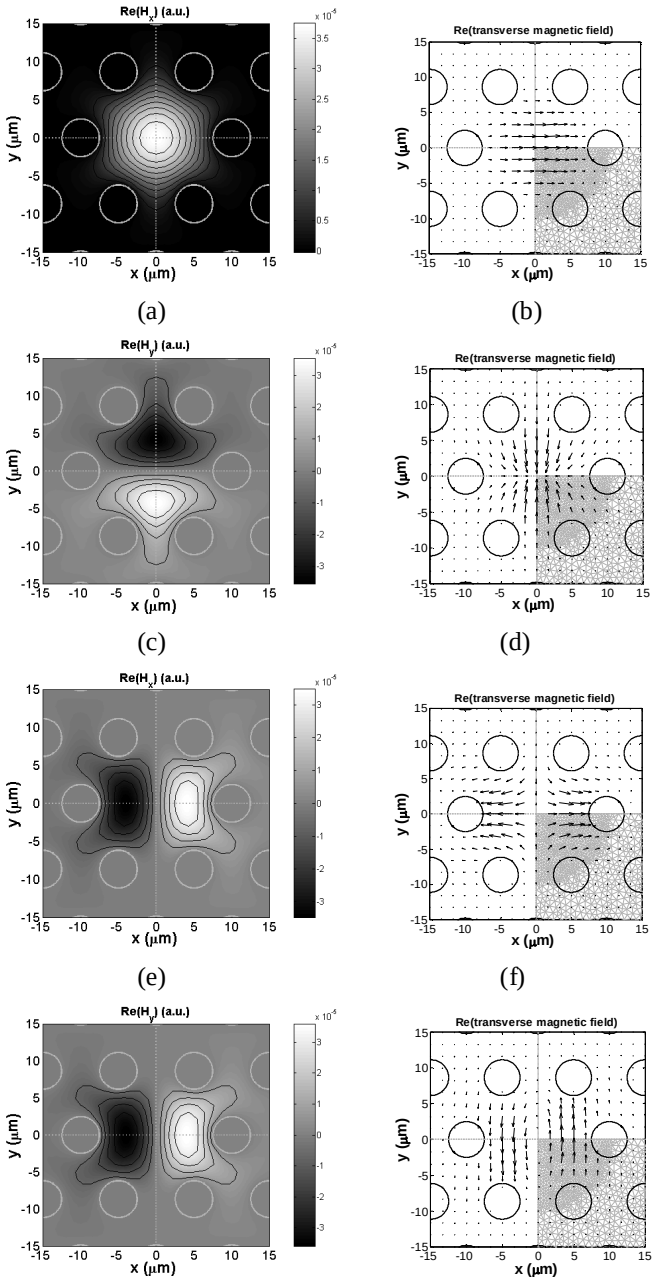

(a) (b) (c) (d) (e) (f) (g) (h)

Fig. 12. Several dominant modes of a commercial PCF. (a) and (b) the q-HE_{11} mode, (c) & (d) the q-TE_{01} mode, (e) & (f) q-HE_{21} mode, and (g) & (h) q-TM_{01} mode. Left column: the dominant magnetic field component of the modes. Right column: the transverse magnetic field vectors.

IV.2. Quasi-guiding Light in Hollow-core Waveguides

During recent years, the interest in (quasi-)guiding light in hollow-core structures, is growing. Initially, their development was driven by the fact that glasses (or other

solid materials suitable for making the fiber) available at that moment, are not transparent in some wavelength range, especially in the UV and mid/far IR regions. Besides, the emergence of high power lasers for industrial and medical applications requires a waveguide with a high damage threshold for power delivery applications. These requirements lead to the development of the hollow fiber [40], [41], which is a fiber with a hollow core and reflective coating(s) at the inner wall. Thereafter, along with the development of the concept of guiding light with the photonic bandgap cladding [42], hollow-core fibers with more complicated cladding structures are developed [43]-[44]. Recently, similar concepts were also proposed for integrated optics by utilizing the ARROW and photonic-bandgap principles [8], [45]-[46]. Nowadays, the potential applications of hollow-core waveguides are not limited to exploiting the high-damage threshold of the hollow waveguides only, but include also high linearity, low loss, and low chromatic dispersion of air which forms the core. Besides, the possibility to fill the holes with gas, liquid, or even particles opens up new applications in the field of light-matter interactions.

IV.2.1. Hollow-core Photonic Bandgap Fibers

Basically, there are 2 groups of hollow-core fibers that utilize the photonic bandgap concept, which are the Bragg fibers and the holey-cladding PBFs. The Bragg fibers are as shown in Fig. 10.(f). They incorporate 1-D periodic concentric bilayers of alternating high and low refractive indices which form a Bragg reflector as cladding [42]. For wavelengths located within the bandgap of this 1-D photonic crystal, modes within the core can't pass through the cladding, and hence are being trapped within the low-index core, which can be just a hollow core. A special type of Bragg fiber that uses an omni-directional reflector as cladding is known as the omni-guide fiber [47] which is widely used as flexible laser scalpel for modern surgery. Besides having the ability to guide light within the air core, the Bragg fibers are interesting since they exhibit lowest loss for TE_{01} mode [48], which is not the fundamental mode of the fiber. This property, which arises from the fact that TE reflection is higher than TM in thin film optics, makes this kind of fiber be particularly interesting since the TE (and also TM) modes in fibers are non-degenerate modes. By exploiting the Brewster angle phenomenon, it is possible to design fibers, which support only a single-mode, without polarization related degeneracy, and which are hence suitable to overcome the polarization mode dispersion (PMD) issues in high-speed fiber optic communications.

The holey-cladding PBFs are fibers with a cladding composed of transverse periodic structure in such a way that modes located within the bandgap of this 2-D photonic crystal can't pass through, hence will be trapped within the core (as the defect), which can be just an air core. Fig. 10.(d)-(f) depicts some examples of these fibers. The first hollow-core guidance by the 2-D photonic bandgap effect was demonstrated by Cregan *et al.* [43]. After that, various cladding structures have been proposed. Those, which exhibit promising results, are mostly with air holes of non-circular shapes in order to achieve the high air-filling fraction which is required to open a wide bandgap [49] on one hand and less surface modes on the other hand. Recently, an air core PBF with air holes in the cladding arranged in a circular arrangement has been demonstrated [44]. This fiber can be viewed as a marriage between the holey cladding PBF and the Bragg fiber.

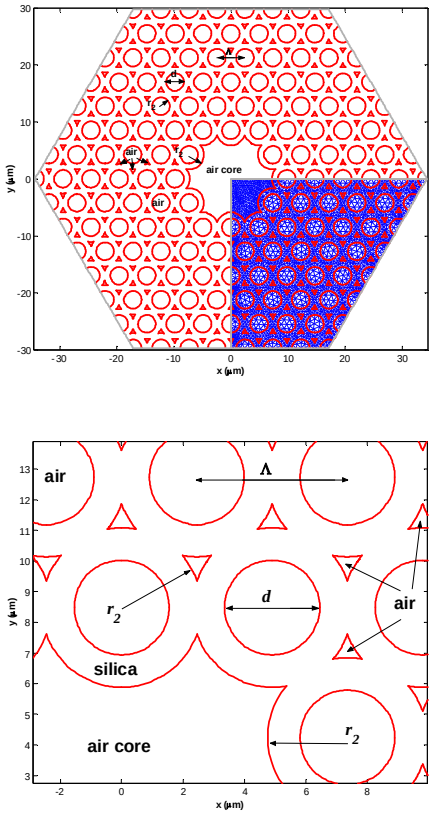

Fig. 13. The structure model used to represent the world's first air-core PBF of Cregan.

As most part of the light is concentrated within the hollow core, the effect of the material loss in these structures is small. Hence, these fibers were initially expected to be able to surpass the lowest-loss limit of the ordinary fiber [5]. However, it is not easy to achieve low structural loss, which is mainly dominated by the scattering due to the fabrication imperfection and the existence of the highly leaky surface modes, which anti-cross with the core modes [50] and introduce extra loss for some wavelength regions, even in the bandgap. Meanwhile, various interesting applications have been demonstrated for these types of fibers, e.g. guiding particles through the air core [9], gas absorption spectroscopy [7], high power [51] and short pulses [52] delivery, gas nonlinear optics [53], etc.

In their practical forms, these fibers have a limited size of the periodic cladding structures. Most of them incorporate a large portion of uniform high index outer cladding in order to get good mechanical strength and size compatibility with the ordinary fiber. Hence, these fibers can also be considered as leaky structures which quasi-guide light simply by defect

resonance principles as demonstrated in following subsections.

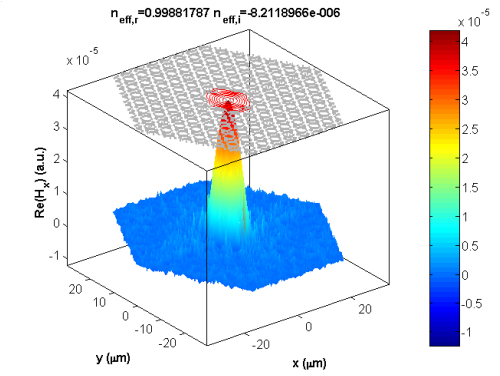

(a)

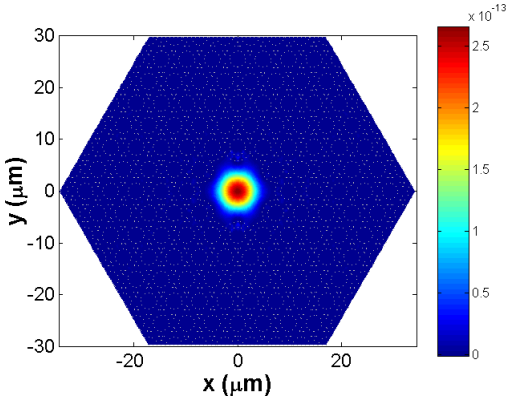

(b)

Fig. 14. The (a). major field component and (b). longitudinal component of time-averaged Poynting vector of HE_{11}-like mode of the world's first air-core PBF.

IV.2.1.1. Air-core photonic bandgap fiber of Cregan

The world's first air-core PBF with 2-D photonic bandgap cladding demonstrated by Cregan *et al.* [43] has a rather complicated structure. We model the fiber with a simplified structure as shown by Fig. 13 [54], which includes the interstitial holes. Here, we have used the 1st-BGT-like TBC to truncate the structure at the fifth and half ring of holes and use only a quarter hexagon with side of 7Λ as our computational domain. Note that the TBC does not represent the periodic (non-uniform) exterior cladding, but instead assumes an element-wise homogeneous extension of the material, hence the computed leakage loss value might be not so meaningful. Fig. 14 shows the computed fundamental mode of the fiber which is qualitatively similar in profile as the one observed in the experiments of Cregan [43].

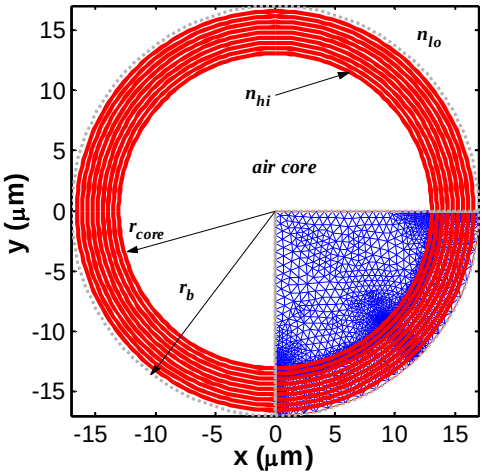

Fig. 15. The air-core Bragg fiber.

IV.2.1.2. Air-core Bragg fiber

As an example of a Bragg fiber, we consider an air-core Bragg fiber with 17 coaxial Bragg layers of alternating high- and low-index materials, starting with the high-index material closest to the core and ending up with low-index material as the outermost cladding as shown in Fig. 15 [54].

The refractive indices of the high-index material n_{hi}, the low-index material n_{lo}, and the air-core are 4.6, 1.6, and 1, respectively for $\lambda = 1.55$ μm. The thicknesses of the high-index layer t_{hi} and the low-index layer t_{lo} are $0.22a$ and $0.78a$, respectively, with period $a = 0.434$ μm. The radius of the air-core is $r_{core} = 13.02$μm. This structure is the same as the one considered also by Johnson *et al.* [47], Basset and Argyros [48], and Zhi *et al.* [55].

Fig. 16 shows the modal field profiles of few dominant (i.e. those with low loss) modes of the structure, computed using a computational domain of a quarter circle with r_b=17μm. Besides these modes, we also observed the existence of other modes, like the so-called surface modes, but their attenuation is higher than TE modes. Fig 16(a) shows that the profile of the dominant field component of HE_{11} mode is eccentric (see e.g. the elliptical shape of the contour plot and the existence of wing-like profile near the left and right inner wall of the Bragg layers). We believe that this phenomenon is induced by the vectorial character of the mode owing to the high index-contrast of the structure, where due to the orientation of the modal field vector, the left-right and top-bottom side of the Bragg layers are not felt to be the same. Of course, due to the symmetry of the structure, there also exists the degenerate pair of this mode, which is oriented in perpendicular direction. We note that similar field eccentricity was also observed by Hadley [56] and Johnson *et al.* [47].

An interesting property of Bragg fiber is that TE_{01} mode, which is not the fundamental mode, is the mode with lowest loss. This can be understood as the electric field of the TE mode is parallel with the surface of the Bragg layers, leading to TE-polarization analogy in a simplified planar

reflection/transmission picture. It is well known that TE-polarized light exhibits higher reflection than TM-polarized light [6]. Therefore, the leakage loss of this TE mode is very low as it does not have TM-polarized component. Utilizing this fact, by carefully design the structure in order to have it operated in the Brewster condition, Basset and Argyros [48] proposed a way to enhance the single-mode single-polarization properties of the Bragg fibers, which might be valuable for future telecommunication applications regarding to the issues of polarization mode dispersion effects.

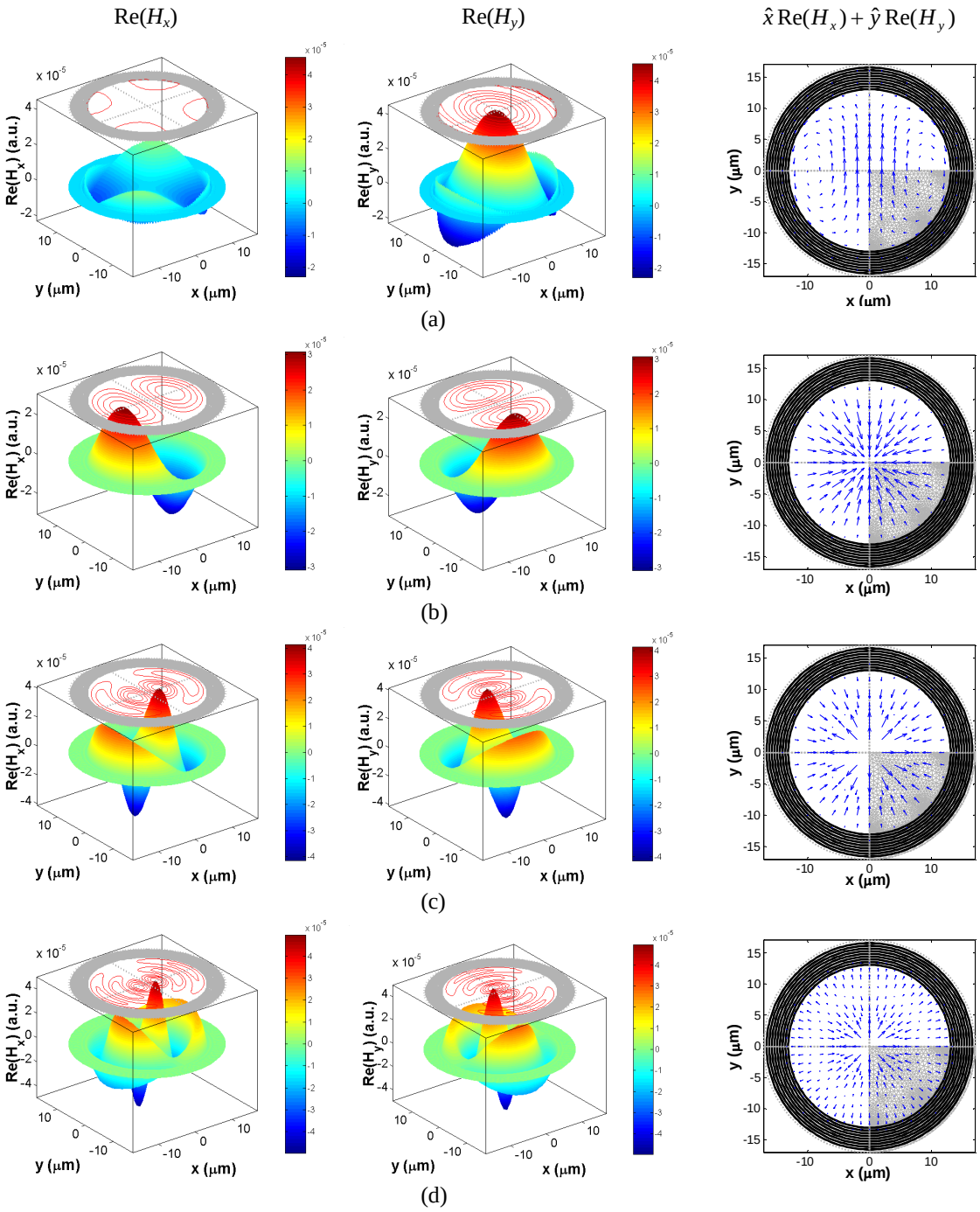

Fig. 16. Mode profile of (a). HE_{11}, (b). TE_{01}, (c). TE_{02}, and (d). TE_{03} modes of the Bragg fiber.

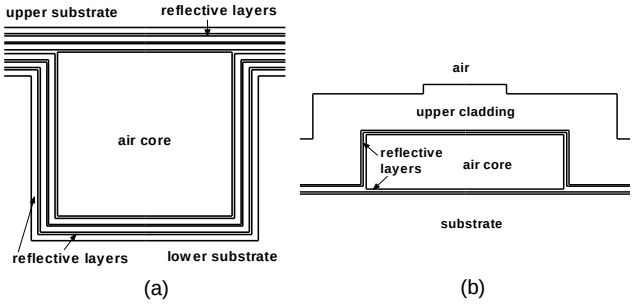

Fig. 17. Examples of cross-section of hollow-core integrated optical waveguides: (a). channel hollow-core waveguide made by wafer bonding, and (b). by the employment of a sacrificial layer. The reflective layer(s) are normally design by applying anti-resonant or omni-directional reflection principles.

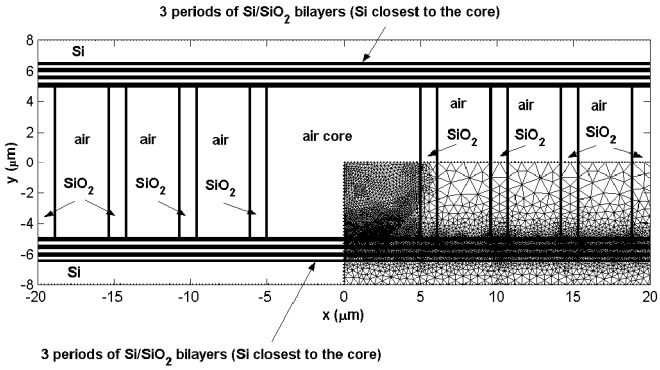

Fig. 18. The proposed low leakage loss hollow-core integrated optical structure and its FEM model.

IV.2.2. Hollow-core Integrated Optical Waveguides

Although quasi-guiding light in low-index core has been employed in integrated optics since a long time ago (see sections IV.1.1 and IV.1.2), the use of hollow core for integrated optics is still in its infancy at this moment. Some possible cross-sections for such structures are depicted in Fig. 17. In general, these structures consist of a hollow core with reflective layer(s) at the inner wall. In the past, the reflective coating itself can be simply a metallic coating. Nowadays, they consist of dielectric bilayers, which are designed to give high reflection for the mode of interest (usually the fundamental mode), such that the power of this mode is trapped within the core. To get the expected high reflection, the ARROW principles and the omni-directional Bragg reflectors are used to design the bilayers.

In 2001, Miura *et al.*, demonstrated a hollow-core waveguiding in a metal coated groove made on a GaAs wafer [57]. Later on, the same group also demonstrated a hollow-core slab waveguide integrated with other optical component(s) such as gratings [58]. Recently, more and more efforts have been put into air core channel integrated optical structures. Yin *et al.* employed a sacrificial layer to demonstrate hollow-core light guidance on a Si wafer as in Fig. 17(b). [45]. Campopiano *et al.* combined a large hollow-core waveguide with a microfluidic system to construct a liquid refractometric sensor [8]. Recently, with the emerging of opto-fluidic systems [59]-[60], hollow-core waveguides are attracting more interests, since they open up many new applications like tunable optical devices [61], optical sensors [8] and integration of bio-electro-optical system into a lab-on-a-chip [62].

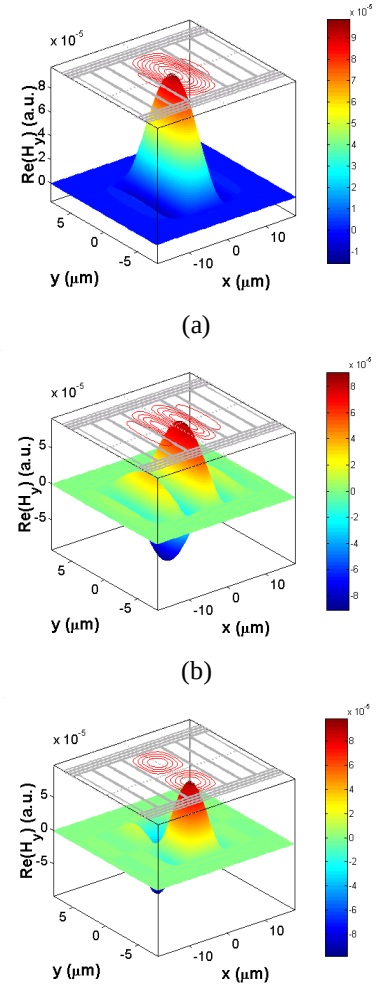

Fig. 19. The dominant component of the magnetic field for q-TE_{00}, q-TE_{10}, and q-TE_{01} modes of the proposed waveguide exhibiting extremely low confinement loss for air-core integrated optical waveguide.

Up to now, there are mainly 2 fabrication methods being used to realize these structures, i.e. the wafer bonding techniques and the use of a sacrificial layer. Due to limitations of the fabrication technologies, the realized structures are usually not as complicated as the PBF. In general, the devices realized by some authors [8], [45] exhibit rather high confinement loss and are hence usable for a simple functionality only. However, once the advancement of the fabrication technologies enables the realization of more complicated structures, and low loss structures can be realized, we believe that this kind of structures would be very interesting, as they allow the integration of various functionalities into a compact chip. Regarding this issue, we proposed a hollow-core integrated optics structure [6] which shows 40 times (in dB scale) lower loss than the so far reported low loss air-core integrated optical waveguides by carefully selecting the materials. Fig. 18 and Fig. 19 show the structure and the dominant modes of waveguide respectively. Although we understand that it is still very difficult to realize the device by current state of the art microstructuring technologies, the material composition considerations that we proposed will seed optimism and be helpful for selection of proper materials in future hollow-core integrated optical waveguides design.

V. Conclusions

The quasi-guiding of light by leaky defect resonance principles are described. A finite element method modeling based on such principles by employing boundary conditions that allow leakage of light through the computational boundaries was developed and implemented. Several leaky channel waveguides were studied and reviewed through the model for its principles, applications, and prospect.

Acknowledgment

The works described in this chapter were mainly supported by the STW (Dutch Applied Technology Foundation) through Project TWI.4813 and TOE.6596 and partly by LPPM of University of Pelita Harapan through project P-011-FTI/IV/2008 and The Directorate General of Higher Education (Dikti), Republic of Indonesia, through Hibah Bersaing project with contract No. 023/K3.KU/2012 (Kopertis Wil. III) followed by contract No. 023/SPHP/LPPM/V/2012 (LPPM UPH). The authors thank Lionix BV for permission to use their test mask and thank M. Dijkstra for fabrication of the waveguide shown in Fig. 1.

References

[1] The quotation mark is used to denote that the structures being considered here do not work in the truly guided-mode regime but in fact in the leaky mode regime. Hence, the term “quasi-guiding” is more appropriate than “guiding” light.

[2] H. P. Uranus, H. J. W. M. Hoekstra, and E. van Groesen, "Finite element and perturbative study of buffered leaky planar waveguides,” *Opt. Commun.*, Vol. 253, No. 1-3, pp. 99-108, 2005.

[3] M. A. Duguay, Y. Kokubun, and T. L. Koch, “Antiresonant reflecting optical waveguides in SiO_2-Si multilayer structures,” *Appl. Phys. Lett.*, Vol. 49, No. 1, pp. 13-15, 1986.

[4] J. C. Knight *et al.*, “All-silica single-mode optical fiber with photonic crystal cladding,” *Opt. Lett.*, Vol. 21, No. 19, pp. 1547-1549, 1996.

[5] P. Russell, “Photonic crystal fibers,” *Science*, Vol. 299, No. 5605, pp. 358-362, 2003.

[6] H. P. Uranus, H. J. W. M. Hoekstra, and E. van Groesen, "Considerations on material composition for low-loss hollow-core integrated optical waveguides,” *Opt. Commun.*, Vol. 260, No. 2, pp. 577-582, 2006.

[7] T. Ritari *et al.*, “Gas sensing using air-guiding photonic bandgap fibers,” *Opt. Express*, Vol. 12, No. 17, pp. 4080-4087, 2004.

[8] S. Campopiano *et al.*, “Microfluidic sensor based on integrated optical hollow waveguides,” *Opt. Lett.*, Vol. 29, No. 16, pp. 1894-1896, 2004.

[9] F. Benabid, J. C. Knight, and P. St. J. Russell, “Particle levitation and guidance in hollow-core photonic crystal fiber,” *Opt. Express*, Vol. 10, No. 21, pp. 1195-1203, 2002.

[10] J. D. Joannopoulos, S. G. Johnson, J. N. Winn, and R. D. Meade, *Photonic crystals: molding the flow of light*, 2nd ed., Princeton Univ. Press, New Jersey, 2008.

[11] H. P. Uranus, *Guiding light by and beyond the total internal reflection principles*, thesis, Univ. Twente, Enschede, 2005.

[12] D. Marcuse, *Theory of dielectric optical waveguides*, Academic Press, New York, 1974.

[13] M. N. O. Sadiku, *Numerical Techniques in Electromagnetics*, 2nd ed., CRC Press, New York, 2001.

[14] A. Bayliss, M. Gunzburger, and E. Turkel, “Boundary conditions for the numerical solution of elliptic equations in exterior regions,” *SIAM J. Appl. Math.*, Vol. 42, No. 2, pp. 430-451, 1982.

[15] H. J. W. M. Hoekstra, J. C. van’t Spijker, and H. M. M. K. Koerkamp, “Ray picture for prism-film coupling,” *J. Opt. Soc. Am. A*, Vol. 10, No. 10, pp. 2226-2230, 1993.

[16] G. Altena *et al.*, “A novel MOEMS device: detection of MEMS movements using free-standing Si_3N_4 suspended optical waveguides,” *Proc. 8th Symposium IEEE LEOS Benelux Chapter*, Enschede, The Netherlands, pp. 25-28, 2003.

[17] R. M. de Ridder *et al.*, “Silicon oxynitride planar waveguiding structures for application in optical communication,” *J. Sel. Topics in Quantum Electron.* Vol. 4, No. 6, pp. 930-937, 1998.

[18] P. Bienstman, S. Selleri, L. Rosa, H. P. Uranus, W. C. L. Hopman, R. Costa, A. Melloni, L. C. Andreani, J. P. Hugonin, P. Lalanne, D. Pinto, S. S. A. Obayya, M. Dems, K. Panajotov, “Modelling leaky photonic wires: a

mode solver comparison," *Opt. and Quantum Electron.*, Vol. 38, No. 9-11, pp. 731-759, July 2006.

[19] H. P. Uranus, "Computational study on modeness of silicon on insulator photonic wire with water cladding," submitted to *The International Conference on Advances Science and Contemporary Engineering 2012 (ICASCE 2012)*, Jakarta, 24-25 Oct. 2012.

[20] K. Benaissa and A. Nathan, "Silicon anti-resonant reflecting optical waveguides for sensor applications," *Sensors and Actuators A*, Vol. 65, No. 1, pp. 34-44, 1998.

[21] J. M. Heaton *et al.*, "Novel 1-to-N way integrated optical beam splitters using symmetric mode mixing in GaAs/AlGaAs multimode waveguides," *Appl. Phys. Lett.*, Vol. 61, No. 15, pp. 1754-1756, 1992.

[22] M. Galarza *et al.*, "1.55μm InP-InGaAsP Fabry-Perot lasers with integrated spot size converters using antiresonant reflecting optical waveguides," *Photon. Technol. Lett.*, Vol. 14, No. 8, pp. 1043-1045, 2002.

[23] T. Baba and Y. Kokubun, "Dispersion and radiation loss characteristics of antiresonant reflecting optical waveguides - numerical results and analytical expressions," *J. Quantum Electron.*, Vol. 28, No. 7, pp. 1689-1700, 1992.

[24] N. M. Litchinitser *et al.*, "Application of ARROW model for designing tunable photonic devices," *Opt. Express*, Vol. 12, No. 8, pp. 1540-1550, 2004.

[25] P. S. Westbrook *et al.*, "Cladding-mode resonances in hybrid polymer-silica microstructured optical fiber gratings," *Photon. Technol. Lett.*, Vol. 12, No. 5, pp. 495-497, 2000.

[26] T. T. Larsen *et al.*, "Optical devices based on liquid crystal photonic bandgap fibres," *Opt. Express*, Vol. 11, No. 20, pp. 2589-2596, 2003.

[27] Although they are widely used in the literature, we will avoid to use the terms "modified total internal reflection" or "index-guiding" to denote this quasi-guiding mechanism, as these terms lead to the notion of lossless guided modes.

[28] T. A. Birks, J. C. Knight, and P. St. J. Russell, "Endlessly single-mode photonic crystal fiber," *Opt. Lett.*, Vol. 22, No. 13, pp. 961-963, 1997.

[29] J. C. Knight *et al.*, "Large mode area photonic crystal fibre," *Electron. Lett.*, Vol. 34, No. 13, pp. 1347-1348, 1998.

[30] J. C. Knight *et al.*, "Anomalous dispersion in photonic crystal fiber," *Photon. Technol. Lett.*, Vol. 12, No. 7, pp. 807-809, 2000.

[31] W. H. Reeves *et al.*, "Demonstration of ultra-flattened dispersion in photonic crystal fibers," *Opt. Express*, Vol. 10, No. 14, pp. 609-613, 2002.

[32] T. A. Birks *et al.*, "Dispersion compensation using single-material fibers," *Photon. Technol. Lett.*, Vol. 11, No. 6, pp. 674-676, 1999.

[33] K. M. Kiang *et al.*, "Extruded singlemode non-silica glass holey optical fibres," *Electron. Lett.*, Vol. 38, No. 12, pp. 546-547, 2002.

[34] A. Michie *et al.*, "Temperature independent highly birefringent photonic crystal fibre," *Opt. Express*, Vol. 12, No. 21, pp. 5160-5165, 2004.

[35] G. Vienne *et al.*, "First demonstration of air-silica Bragg fiber," post deadline paper PDP25, *Optical Fiber Conf. 2004*, Los Angeles, 22-27 Feb. 2004.

[36] H. P. Uranus, H. J. W. M. Hoekstra, and E. van Groesen, "Modes of an endlessly single-mode photonic crystal fiber: a finite element investigation," *Proc. Annual Symposium IEEE LEOS Benelux Chapter*, Ghent, 2-3 Dec. 2004.

[37] J. A. West *et al.*, "Surface modes in air-core photonic band-gap fibers," *Opt. Express*, Vol. 12, No. 8, pp. 1485-1496, 2004.

[38] http://www.nktphotonics.com.

[39] H. P. Uranus, "Theoretical Study on the Multimodeness of a Commercial Endlessly Single-Mode PCF," *Opt. Commun.*, Vol. 283, pp. 4649-4654, 2010.

[40] J. A. Harrington, "A review of IR transmitting hollow waveguides," *Fiber and Integrated Opt.*, Vol. 19, No. 3, pp. 211-227, 2000.

[41] H. Jelinkova *et al.*, "Hollow waveguide delivery systems for laser technological application," *Prog. Quantum Electron.*, Vol. 28, pp. 145-164, 2004.

[42] P. Yeh, A. Yariv, and E. Marom, "Theory of Bragg fiber," *J. Opt. Soc. Am.*, Vol. 68, No. 9, pp. 1196-1201, 1978.

[43] R. F. Cregan *et al.*, "Single-mode photonic band gap guidance of light in air," *Science*, Vol. 285, No. 5433, pp. 1537-1539, 1999.

[44] G. Vienne *et al.*, "First demonstration of air-silica Bragg fiber," post deadline paper PDP25, *Optical Fiber Conf. 2004*, Los Angeles, 22-27 Feb. 2004.

[45] D. Yin *et al.*, "Integrated ARROW waveguides with hollow cores," *Opt. Express*, Vol. 12, No. 12, pp. 2710-2715, 2004.

[46] Y. Yi *et al.*, "On-chip Si-based Bragg cladding waveguide with high index contrast bilayers," *Opt. Express*, Vol. 12, No. 20, pp. 4775-4780, 2004.

[47] S. G. Johnson *et al.*, "Low-loss asymptotically single-mode propagation in large-core OmniGuide fibers," *Opt. Express*, Vol. 9, No. 13, pp. 748-779, 2001.

[48] I. M. Bassett and A. Argyros, "Elimination of polarization degeneracy in round waveguides," *Opt. Express*, Vol. 10, No. 23, pp. 1342-1346, 2002.

[49] N. A. Mortensen and M. D. Nielsen, "Modeling of realistic cladding structures for air-core photonic bandgap fibers," *Opt. Lett.*, Vol. 29, No. 4, pp. 349-351, 2004.

[50] K. Saitoh, N. A. Mortensen, and M. Koshiba, "Air-core photonic band-gap fibers: the impact of surface modes," *Opt. Express*, Vol. 12, No. 3, pp. 394-400, 2004.

[51] B. Temelkuran *et al.*, "Wavelength-scalable hollow optical fibres with large photonic bandgaps for CO_2 laser transmission," *Nature*, Vol. 420, No. 6916, pp. 650-653, 2002.

[52] G. Humbert *et al.*, "Hollow core photonic crystal fibers for beam delivery," *Opt. Express*, Vol. 12, No. 8, pp. 1477-1484, 2004.

[53] F. Benabid *et al.*, "Stimulated Raman scattering in hydrogen-filled hollow-core photonic crystal fiber," *Science*, Vol. 298, No. 5592, pp. 399-402, 2002.

[54] H. P. Uranus, "Serat optik dengan inti udara: studi komputasional," *Proc. Seminar Nasional Forum Teknik Elektro Indonesia 2011 (FORTEI 2011)*, Makassar, Indonesia, 8-9 Dec. 2011, pp. 143-144.

[55] W. Zhi *et al.*, "Compact supercell method based on opposite parity for Bragg fibers," *Opt. Express*, Vol. 11, No. 26, pp. 3542-3549, 2003.

[56] G. R. Hadley, "Numerical simulation of waveguides of arbitrary cross-section," *Int. J. Electron. Commun. (AEU)*, Vol. 58, No. 2, pp. 86-92, 2004.

[57] T. Miura *et al.*, "Hollow optical waveguide for temperature-insensitive photonic integrated circuits," *Jpn. J. Appl. Phys.*, Vol. 40, No. 7A, pp. L688-L690, 2001.

[58] Y. Sakurai and F. Koyama, "Tunable hollow waveguide distributed Bragg reflectors with variable air core," *Opt. Express*, Vol. 12, No. 13, pp. 2851-2856, 2004.

[59] D. Psaltis, S. R. Quake, and C. Yang, "Developing optofluidic technology through the fusion of microfluidics and optics," *Nature*, Vol. 442, pp. 381-386, 2006.

[60] C. Monat, P. Domachuk, and B. J. Eggleton, "Integrated optofluidics: A new river of light," *Nat. Photonics*, Vol. 1, pp. 106-114, 2007.

[61] Z. Li, Z. Zhang, T. Emery, A. Scherer, and D. Psaltis, "Single mode optofluidic distributed feedback dye laser," *Opt. Express*, Vol. 14, No. 2, pp. 696-701, 2006.

[62] A. van den Berg and P. Bergveld, "Labs-on-a-chip: origin, highlights and future perpectives – On the occasion of the 10th μTAS conference," *Lab on a Chip*, Vol. 6, pp. 1266-1273, 2006.